OPEN ACCESS
IOP Publishing
Plasma Physics and Controlled Fusion
Plasma Phys. Control. Fusion **66** (2024) 055012 (9pp)
https://doi.org/10.1088/1361-6587/ad349b

Identifying quantum effects in seeded QED cascades via laser-driven residual gas in vacuum

Yinlong Guo[1,2], Xuesong Geng[1], Liangliang Ji[1,*], Baifei Shen[3] and Ruxin Li[1,4,*]

[1] State Key Laboratory of High Field Laser Physics and CAS Center for Excellence in Ultra-intense Laser Science, Shanghai Institute of Optics and Fine Mechanics (SIOM), Chinese Academy of Sciences (CAS), Shanghai 201800, People's Republic of China
[2] Center of Materials Science and Optoelectronics Engineering, University of Chinese Academy of Sciences, Beijing 100049, People's Republic of China
[3] Shanghai Normal University, Shanghai 200234, People's Republic of China
[4] ShanghaiTech University, Shanghai 201210, People's Republic of China

E-mail: jill@siom.ac.cn, ruxinli@mail.siom.ac.cn and xsgeng@siom.ac.cn

Received 9 November 2023, revised 3 March 2024
Accepted for publication 15 March 2024
Published 3 April 2024

Abstract

The discrete and stochastic nature of the processes in the strong-field quantum electrodynamics (SF-QED) regime distinguishes them from classical ones. An important approach to identifying the SF-QED features is through the interaction of extremely intense lasers with plasma. Here, we investigate the seeded QED cascades driven by two counter-propagating laser pulses in the background of residual gases in a vacuum chamber via numerical simulations. We focus on the statistical distributions of positron yields from repeated simulations under various conditions. By increasing the gas density, the positron yields become more deterministic. Although the distribution stems from both the quantum stochastic effects and the fluctuations of the environment, the quantum stochastic effects can be identified via the width of the distribution and the exceptional yields, both of which are higher than the quantum-averaged results. The proposed method provides a statistical approach to identifying the quantum stochastic signatures in SFQED processes using high-power lasers and residual gases in the vacuum chamber.

Keywords: strong-field quantum electrodynamics, seeded cascade, quantum stochastic signature, Monte-Carlo simulation

1. Introduction

High-intensity lasers can provide extreme conditions as a powerful tool for plasma-based accelerators and novel radiation sources [1–4]. It is expected that the focal intensities of 10–100 PW class lasers could approach beyond 10^{23} W cm^{-2}, where strong-field quantum electrodynamics (SF-QED) processes play significant roles [5–12], such as gamma photon radiation [5], radiation reaction [13], Breit–Wheeler (BW) pair-production [14], spin polarization [15, 16] and QED cascades [17–23]. Among the SF-QED processes, the stochastic effects are prominent signatures that depict the quantum nature of the SF-QED theories, which can be observed in the change of electron energy [24–27], trajectory [28–31], photon emission [32, 33] or spin [34]. These have drawn particular attention in theoretical [7, 15, 27–29, 32] and experimental [35–38] studies over the decades.

Spontaneous electron-positron pair creation out of the vacuum can take place when the field strength is higher than the Sauter–Schwinger critical field $E_S \approx 1.3 \times 10^{16}\,\mathrm{V\,cm^{-1}}$ [39]. In strong laser fields, pair creation can be triggered at

* Authors to whom any correspondence should be addressed.

a much lower field strength [5, 40]. When the field strength is sufficiently strong, electron-positron pairs which will emit photons capable of decaying into new pairs, leading to QED cascades. It has been shown that the onset of seeded cascade (with one electron at the beginning) can be facilitated at an intensity around 10^{24} W cm^{-2} [18–20, 41]. Electron-positron plasma can be exponentially generated via self-sustained gamma photon radiation and pair-production with even one electron in the propagating or standing wave formed by ultra-intense laser pulses [17, 18, 21]. As the plasma density grows, the laser can eventually be absorbed [42], which determines the upper limit of the strong field in a non-ideal vacuum [17, 43]. Since seeded QED cascades couple both the stochasticity of photon radiation and pair-production, a strong quantum nature emerges. For instance, the positron yield is stochastic in a non-ideal vacuum setup [20, 21].

In this article, we are going to show that the positron yields in seeded QED cascades can be a convenient signal to identify the stochasticity of QED cascades. The statistical distribution of the yields among multiple simulations conforms to a specific distribution, the width of which is larger than that of the photon radiation alone (without coupling) and much larger than the QED-average/semi-classical results. This signature indicates the stochastic nature of QED cascades and the coupling effect of photon radiation and pair-production. The cascade can be triggered by the residual gas in vacuum chambers without the need to fix or inject electrons at the laser focuses, which can potentially test the strong-field theory in the 100 PW-class laser systems [1, 3, 4]. The quantum stochastic effects of QED cascades can be identified by evaluating the positron yield distribution of multiple laser shots hitting the residual gas through a statistical method.

2. Methods

2.1. QED Monte-Carlo cascades

The two basic QED processes, nonlinear Compton scattering (NCS) and nonlinear BW process, play the most important roles in QED cascades. Under the assumption of a strong field, the instantaneous photon emission rate is [5, 44]:

$$\frac{\mathrm{d}^2 N_\gamma}{\mathrm{d}\tau \mathrm{d}\gamma_\gamma} = \frac{\sqrt{3}}{3\pi}\frac{\alpha_\mathrm{f}}{\gamma_\mathrm{e}^2 \tau_\mathrm{c}}\left[\int_{2y}^{+\infty} K_{\frac{1}{3}}(s)\,\mathrm{d}s - (2+3\chi_\gamma y)\,K_{\frac{2}{3}}(2y)\right], \tag{1}$$

where $\alpha_\mathrm{f} \approx 1/137$ the fine structure constant, γ_e the electron relativistic factor, $\tau_\mathrm{c} = \frac{\hbar}{m_\mathrm{e}c^2}$, $\hbar$ the reduced Planck constant, m_e the electron mass, c the speed of light, $\chi_\mathrm{e} = \left|\frac{F^{\mu\nu}}{E_\mathrm{s}}\frac{p_\nu}{m_\mathrm{e}c}\right|$ and $\chi_\gamma = \left|\frac{F^{\mu\nu}}{E_\mathrm{s}}\frac{\hbar k_\nu}{m_\mathrm{e}c}\right|$ the Lorentz-invariant quantum parameter of the electron and the photon, $F^{\mu\nu}$ the electromagnetic field tensor, p_ν the electron four-momentum (the photon four-momentum $\hbar k_\nu$) and $E_\mathrm{S} \approx 1.32\times10^{18}\,\mathrm{V\,m^{-1}}$ the Sauter–Schwinger critical field [39]. $K_{\frac{1}{3}}(s)$, $K_{\frac{2}{3}}(y)$ the modified Bessel functions and $y = \frac{\chi_\gamma}{3\chi_\mathrm{e}(\chi_\mathrm{e}-\chi_\gamma)}$, respectively. Similarly, the rate of photons decaying into $\mathrm{e}^+\mathrm{e}^-$ pairs is [5, 44]:

$$\frac{\mathrm{d}^2 N_\pm}{\mathrm{d}\tau \mathrm{d}\gamma_\mathrm{e}} = \frac{\sqrt{3}}{3\pi}\frac{\alpha_\mathrm{f}}{\gamma_\gamma^2 \tau_\mathrm{c}}\int_{2y}^{+\infty}\sqrt{y}K_{\frac{1}{3}}(s)\,\mathrm{d}s - (2-3\chi_\gamma y)\,K_{\frac{2}{3}}(y), \tag{2}$$

where γ_e is the relativistic factor of the newborn electron, and γ_γ the photon relativistic factor.

For the commonly used codes to simulate interactions with QED processes, the point-like QED events take place on the classical trajectory and are implemented by the Monte-Carlo method [44–46] in each time step. Each electron is randomly assigned an optical depth which decreases according to the radiation probability rate and the radiation event is triggered when the optical depth decreases below zero. The photon energy is then determined via inverse sampling of the photon spectrum equation (1). BW pair production follows a similar process where photons decay into pairs of electrons and positrons.

2.2. QED-averaged cascades

For the purpose of clarifying the quantum stochastic effects, a QED-averaged estimation of positron yield during cascades [17, 21, 40, 42] is carried out. By using the analytical growth rate of the seeded cascade, the differences between QED-MC and QED-averaged cascades can then be attributed to the stochastic effects of QED and it can decouple the extra randomness of the seeded electrons' initial distribution. The growth rate of pairs in a cascade induced by two linear polarized laser pulses has an empirical fit of [42]:

$$\Gamma \sim \frac{8}{15\pi}\left(\frac{2\pi}{3}\right)^{\frac{1}{4}}\frac{\alpha}{\tau_\mathrm{c}\bar{\gamma}}K_{\frac{1}{3}}^2\left(\frac{4}{3\bar{\chi}_\mathrm{e}}\right) \tag{3}$$

where $\alpha \approx \frac{e^2}{\hbar c}$ with e the electron charge, $K_{\frac{1}{3}}$ the modified Bessel function and $\bar{\gamma} \cong \mu^{\frac{3}{4}}\sqrt{a_\mathrm{S}}$, $\bar{\chi}_\mathrm{e} \cong 1.24\mu^{\frac{3}{2}}$ with $\mu = \frac{a}{\alpha a_\mathrm{s}}$. Here $a = \frac{eE}{m_\mathrm{e}\omega_0 c}$ is the normalized laser amplitude with E being the peak electric field, ω_0 the laser angular frequency and $a_\mathrm{S} = \frac{eE_\mathrm{S}}{m_\mathrm{e}\omega_0 c}$. The number of pairs produced by a single electron can then be estimated by $N_\pm \sim e^{\Gamma t} - 1$. In the standing wave formed by two collision laser pulses, the peak field strength experienced by electrons near the collision plane can be approximated by $f_a(r_i) = a_0 e^{-r_i^2/w_0^2}$ with r_i the initial radial position. For N_seed electrons distributed at different r_i, the final electron-positron yield is therefore altered by r_i:

$$N_\pm = \sum_{i=0}^{i=N_\mathrm{seed}}\left[e^{\Gamma(r_\mathrm{i})t_\mathrm{eff}} - 1\right]. \tag{4}$$

The parameter t_eff is inferred from the QED-MC results for consistency consideration by equating $N_\pm$ with the mean yield of 1000 QED-MC results.

2.3. Test-particle simulation

Obtaining the distribution of the positron yields requires thousands of repetitive simulations of QED cascades. It is computationally expensive to carry out particle-in-cell (PIC) simulations. Therefore, a test-particle simulation is adopted.

The test-particle algorithm solves the Lorentz equation with the Boris pusher and simulates photon emission and pair-production with Monte-Carlo method, which is adopted by most QED-PIC codes. Unlike PIC, which solves the Maxwell equations in gridded space and interpolates fields onto shaped macro-particles, the test-particle algorithm evaluates the electromagnetic fields at instantaneous particle positions according to predefined laser profiles. We adopt the focused Gaussian pulses [47] in our calculations, which are linearly polarized (LP) along the y-direction and propagate along the x-direction with a wavelength of $\lambda = 800$ nm. Since the test-particle algorithm ignores the interaction between particles, simulation parameters such as pulse length and field strength are controlled at the onset of the QED cascade region where the number of generated electron-positron pairs is not too high and a large number of simulations is possible. In such situations, collective plasma effects can be ignored due to the relatively low plasma density. In the following simulations, we choose a field strength of $a_0 = 700$, spot size of $w_0 = 4\,\mu$m and pulse length of $\tau_L = 4T_0$, where w_0 and τ_L corresponds to the $1/e$ of the Gaussian profile. The simulation time step is $dt = \frac{T_0}{100}$, which is proved to be sufficient to model NCS and BW processes in the parameter region [45]. We chose a relatively small spot size and short pulse length to suppress further exponential growth of produced pairs [19, 22] for computational consideration. According to our findings to be presented, longer or larger pulses will both result in stronger stochastic signatures.

3. Result

3.1. Fixed seeded electrons

We start from the simplest situation where two colliding LP laser pulses with electrons are fixed at the origin to demonstrate the quantum stochastic effects and statistic scaling law in QED cascades. More realistic considerations will be discussed later. The evolution of the positron yields for a different number of seeded electrons $N_{\rm seed}$ =1, 10, 100, 1000 is shown in figure 1. One can see that although each set of simulations has the same initial condition, the growth and final yields may significantly differ from each other when the number of seeds is low, indicating the quantum stochastic feature of the QED cascades [21]. It should be noted that for $N_{\rm seed} = 1$ cascades are not triggered in most simulations for the considered parameters, and the positron yields distribution gathers near zero. By increasing the number of seeded electrons, the positron yield coverages near the mean value $\bar{N}$ marked by the dashed-lines, indicating a more deterministic behavior of the QED cascades. One can find that $\bar{N}$ increases almost linearly with $N_{\rm seed}$ in statistics, which could be modeled by the analytical calculation [21, 42].

Another noticeable feature is the exceptional positron yields that significantly exceed the mean yield and other results, as indicated in figure 1. For $N_{\rm seed} = 1$ some simulations generate more than 50 positrons and one simulation generates about ∼100 positrons, much larger than the mean value at about $\bar{N} \approx 7$. As $N_{\rm seed}$ increases, such a deviation is significantly depressed, and the statistics become more deterministic,

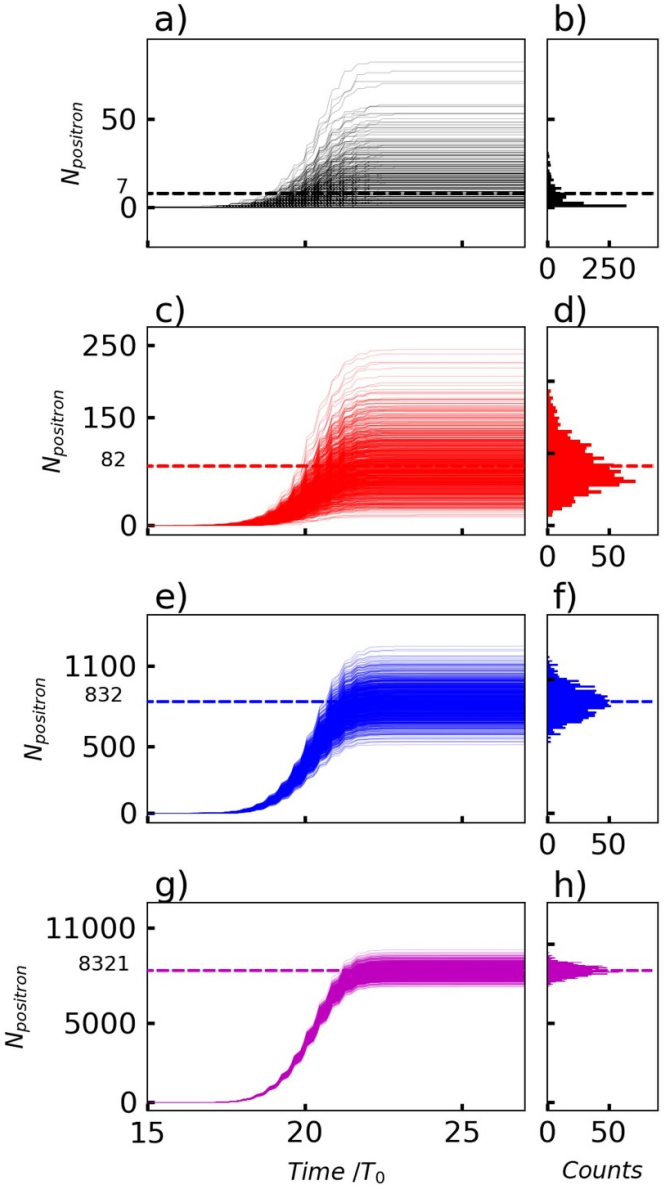

Figure 1. The evolution of the number of positrons (the BW pairs) of 1000 independent simulations with $a_0 = 700$, $\tau_0 = 4T_0$, $w_0 = 4\,\mu$m and their statistic distribution for (a), (b) $N_{\rm seed} = 1$, (c), (d) 10, (e), (f) 100 and (g), (h) 1000. The mean value $\bar{N}$ is marked by dashed lines.

as shown by figures 1(g) and (h). It can be predicted that the QED cascades triggered by thin foil [42, 48, 49] or gases of moderate density [19, 22, 50] are much more predictable and the exceptional yields will be absent.

The positron yield distribution and the exceptional shots reflect the quantum/stochastic nature of photon radiation, radiation-reaction, pair-production, and their coupling. It requires a certain probability for electrons/positrons to emit high-energy photons and for those photons to decay into pairs at specific phases, resulting in abundant positron yields that stem from a sequence of incessant improbable QED events. It should be emphasized that individual photon radiation or pair-production does not lead to similar effects, which will be discussed later.

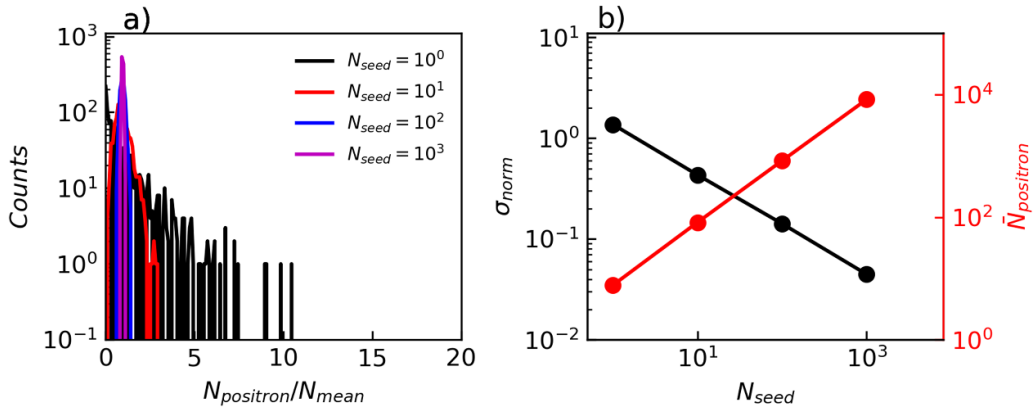

Figure 2. (a) The positrons' yield distribution of 4 sets of simulations ($N_{\rm seed}$ =1, 10, 100, 1000), each of which is normalized by the mean yield of 1000 independent simulations. (b) The normalized distributions' standard deviation σ (black dots) and mean yield $\bar{N}$ (red dots) versus the number of seed $N_{\rm seed}$.

To quantitatively describe the quantum effects, the normalized positron yield distributions are illustrated in figure 2(a). The relative width of the distribution can be modeled by the standard deviation σ which is shown in figure 2(b) along with the mean yield $\bar{N}$. For $N_{\rm seed} = 1$, the distribution displays the strongest quantum stochasticity, wherein cascading is not triggered in most simulations, but it produces a maximum yield that is ten times greater than the mean yield. As $N_{\rm seed}$ increases, both the relative widths and exceptional yields shrink and the statistic distributions become more concentrated and deterministic, as shown by the black-dotted line in figure 2(b). This can be interpreted as the transition of the statistics from quantum to classical, where each particle exhibits its quantum behaviour but the statistics of the particle system behaves more classically as the particle number increases. It should be noted that photon radiation and pair-production are quantum processes with no analogy in classical physics, but the statistics can be deterministic and classical. At the same time, $\bar{N}$ increases linearly to $N_{\rm seed}$ as expected, following equation (4), which models the quantum-averaged positron yields.

The above results reflect the quantum stochastic nature of the coupling between the photon radiation and pair-production as mentioned before, and individual photon radiation or pair-production processes will not induce stronger stochasticity. The normalized photon yields of seed electrons without BW pair production are shown in figure 3 that presents the individual stochasticity of photon radiation. The photon yield distributions are more concentrated than the results in figure 2, indicating lower uncertainty of the individual processes. In cascades, the number and energy of photons radiated by electrons are distributed in a wide range, which will induce a wider distribution of the pairs produced by these photons. The uncertainty of photon radiation and pair-production are then coupled and exhibit higher stochasticity.

On the other hand, the quantum stochastic effects can be further coupled with the classical stochastic accelerations [51], in which the particle's stochastic acceleration is triggered by the random-walk-like motion (wandering path) in the standing wave. These classical effects are naturally included in the

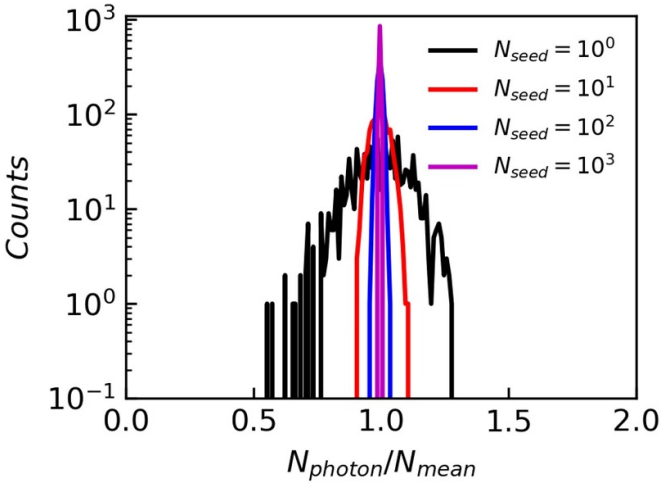

Figure 3. The normalized photons' yield distribution without BW pair production.

calculation by solving the Lorentz equation, which are then imprinted to the radiated photons. As the number of seeding particles increases, the positron yield converges, denoting the limit of classical stochasticity. It is also interesting that the stochastic photon emission could reduce the classical stochastic heating, which could contribute to the existence of attractors in the phase space and even show a transition from chaotic to regular dynamics as the field strength increases [8, 50, 52, 53].

3.2. *Experimental considerations*

Increasing the number of fixed seeded electrons in the focus is only an analog of the transition from quantum statistics to classical statistics, which is not experimentally possible. Previous studies have focused on injecting high-energy seed particles into the strong laser fields to initiate the cascades [41, 54, 55], but this is also challenging to achieve in practice. Here we propose a different approach, where we use the low-density residual gas in the vacuum chamber as the seed particles.

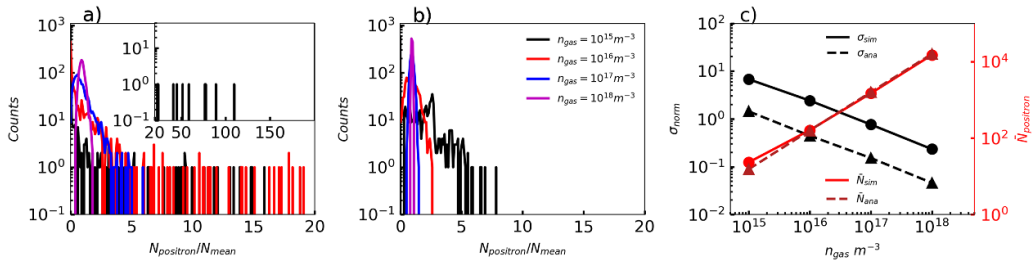

Figure 4. (a) The positrons' yield distributions of 4 sets of simulations ($n_{\rm gas} = 10^{15}$, 10^{16}, 10^{17}, $10^{18}{\rm m}^{-3}$), each of which is normalized by the mean yield $\bar{N}$. (b) The positrons' yield distributions of the semi-classical calculations that only consider the randomness of the initial electron locations. (c) The normalized standard deviation σ (black) and the mean yield $\bar{N}$ (red) versus the gas density $n_{\rm gas}$, where the solid-dotted lines are from simulations and the dashed-triangle lines are from semi-classical (QED-averaged) calculations.

In our modeling, the gas molecules (100% N_2 for simplicity) are pre-ionized by the strong laser fields and randomly distributed around the laser focal area. The electrons of N_2 are randomly distributed in the simulation box of $48\,\mu{\rm m} \times 60\,\mu{\rm m} \times 60\,\mu{\rm m}$ and the number of electrons is determined by the gas number density $n_{\rm gas}$ (or vacuity) and the volume of the interaction region. The counter-propagating laser pulses enter the interaction region from opposite sides of the simulation box along $+x$ and $-x$ direction and trigger cascading.

We simulate seeded cascades with four different gas densities $n_{\rm gas} = 10^{15}, 10^{16}, 10^{17}, 10^{18}{\rm m}^{-3}$, in which $n_{\rm gas} = 10^{15}{\rm m}^{-3}$ is close to the lowest attainable vacuity of the vacuum chamber for PW laser facilities. Figure 4(a) shows the normalized positron yield distribution for 1000 simulations. For low gas densities ($\leqslant 10^{17}{\rm m}^{-3}$) the exponential distribution shows a strong stochastic signature since cascades in most simulations are not initiated due to the low densities. The highest yield is as high as $\frac{N_{\rm positron}}{N_{\rm mean}} > 100$ at $n_{\rm gas} = 10^{15}{\rm m}^{-3}$, much higher than the fixed seeded electrons, since the mean yield of low-density gas is lower than that of the fixed electrons. At higher density ($\sim 10^{18}{\rm m}^{-3}$) the statistic distribution shows a classically convergent trend, similar to the results in figure 2(a).

However, the high yield at low densities originates from the additional stochasticity induced by the randomness of the initial distribution of the electrons. For the sole estimation of this aspect, the semi-classical (QED-averaged cascade) results, as introduced in the methods section, are shown in figure 4(b) where the stochastic effects from QED are averaged and the yield distribution can be solely attributed to the randomness of the initial electron locations. By comparing the widths of the distributions in figures 4(a) and (b), we find that the location-induced randomness is significantly lower than the QED-induced randomness. The widths σ and mean yields $\bar{N}$ are compared in figure 4(c), where the mean yields of the QED and QED-averaged results coincide but the widths of the yield distribution of the latter are one-order-of-magnitude lower than the former, indicating that the strength of QED stochasticity exceeds the randomness of initial distribution of the locations and that the gap inbetween represents the stochasticity of QED.

Therefore, two experimental signatures can provide proof of quantum stochastic effects: (1) the statistical distribution and the transition of statistics from quantum stochastic to classical, derived from the interaction between the coupling stochastic effects of quantum nature and the statistically convergent effect induced by multiple seeds. The QED-induced distribution is distinctly different and broader than the semi-classical/QED-averaged calculation; (2) the exceptional prolific shots with much higher yield than the mean expectation for thin gas, where few pairs should be produced in semi-classical/QED-averaged calculations. The yield may be two orders higher than the mean value, thus it can be easily identified by statistical methods.

Considering that 1000 shots is a heavy task for high-power (>100 PW) laser systems due to their low repetition rates, we estimate the minimum required shots to reproduce the distribution of the deviation σ. As shown in figure 5, the black lines represent the widths of yields of QED (solid line) and QED-averaged (dashed line) results for $N_{\rm shots} = 1000$, and the same in figure 4(c), and the shaded areas represent the 5% and 95% percentiles of possible σ that can be observed for shot numbers of $N_{\rm shots} = 10$ (gray), 50 (red) and 100 (green). For very few shots like $N_{\rm shots} = 10$, it is more probable to produce zero-results at low gas densities and the possible σ can be lower than expected. It should take more than 100 shots to resolve the statistical deviation at low density. As the gas density increases, the percentile area shrinks rapidly for both the QED and QED-averaged results, i.e. the transition to classical. The QED results can be well distinguished from the QED-averaged results for $N_{\rm shots} \geqslant 50$. Therefore, more than 50 shots are required to capture the accurate deviation of positron yields and the transition from quantum to classical as the gas density increases.

4. Discussions

4.1. The optimal laser parameter

Here, we estimate the stability of the statistical law for three densities $n_{\rm gas} = 10^{16}, 10^{17}, 10^{18}{\rm m}^{-3}$ with different laser parameters, in order to find the optimal experimental conditions

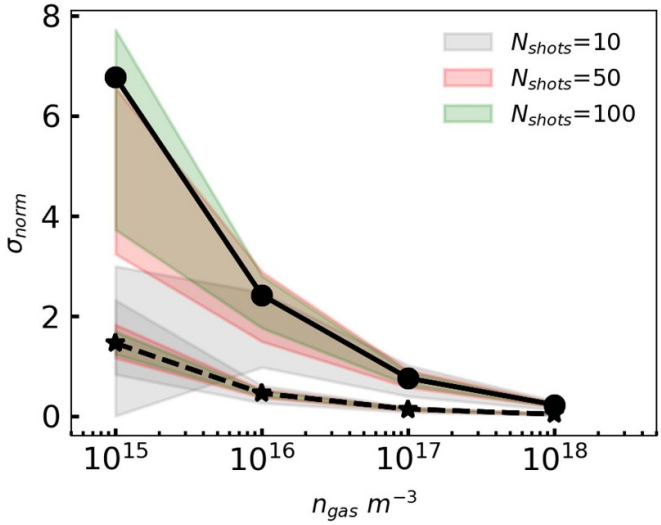

Figure 5. The standard deviation σ of normalized positron yields at different densities $n_{\rm gas}$ for limited number of laser shots of $N_{\rm shots} = 10$ (gray), 50 (red) and 100 (green). The lines are the results of $N_{\rm shots} = 1000$, same in figure 4(c). The shaded areas represent the 5% and 95% percentiles of possible σ of $N_{\rm shots}$ shots.

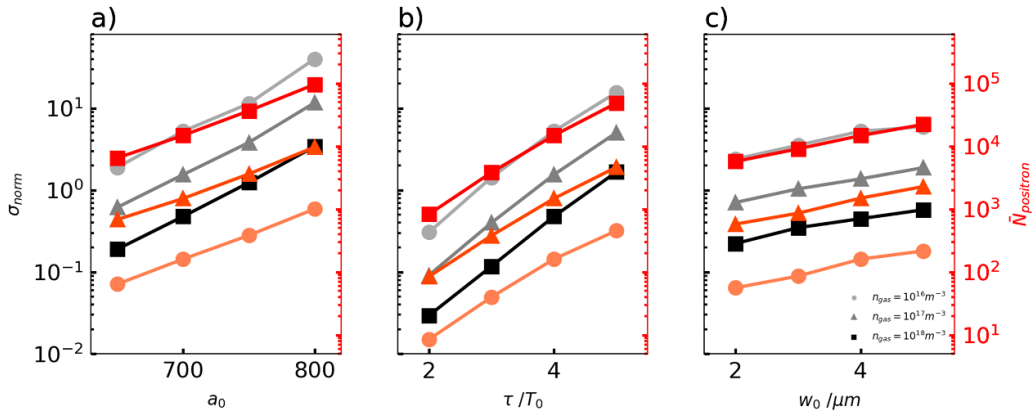

Figure 6. The influence on normalized distributions' standard deviation σ and mean yield $\bar{N}$ for different laser parameters: (a) a_0 varies with $\tau_0 = 4T_0$, $\rm w_0 = \ 4\,\mu m$, (b) τ_0 varies with $a_0 = 700$, $\rm w_0 = \ 4\,\mu m$, (c) w_0 varies with $a_0 = 700$, $\tau_0 = 4T_0$, for each parameter three gas densities $\rm n_{gas} = 10^{16}$, 10^{17}, $10^{18} m^{-3}$ are tested, and each point represents the statistical value of 1000 simulations.

for detection. We consider realistic parameters for near-future experiments: (a) a_0 varies from 650 to 800 and $\tau_0 = 4T_0$, $\rm w_0 = \ 4\,\mu m$, (b) τ_0 varies from $2T_0$ to $5T_0$ and $a_0 = 700$, $\rm w_0 = 4\,\mu m$, (c) $a_0 = 700$, $\tau_0 = 4T_0$ with w_0 varies from $2\,\mu$m to $5\,\mu$m. The results are shown in figure 6 for three gas densities.

In general, increasing a_0, τ_0 or w_0 all lead to higher mean yield of cascades (red lines), which means more QED events, and more significant stochastic features can be observed. This can be verified by the gray lines. It is worth noting that increasing w_0 increases the number of electrons in the colliding volume, which is equivalent to increasing the gas density. On the other hand, it increases the interaction time of cascades in laser fields, which is similar to increasing the pulse length. As already shown in figures 5 and 6(b), the dependence of σ on gas density and pulse length are opposite. As a result, σ shows relatively weak dependence on w_0 as shown by the gray lines in figure 6(c).

Therefore, tightly focused lasers are preferable for the observation of the stochastic effects of QED cascades. This is different from [19, 22] that for optimal cascade development a larger laser spot size is needed. The pulse lengths and field strengths are constrained in the selected region for computational consideration. Predictions can be extrapolated from the results for longer pulse lengths and lower field strengths accessible in future 100 PW-class laser systems [1–4].

4.2. The effect of laser pointing instability

Studies have shown that the time delay between the pulses has a minor impact on the cascades, but the transverse mismatch between pulses can prevent cascading [22]. Taking into consideration the pointing instability, we assume that each pulse has an independent offset Δ in each transverse direction (y and z) that follows $\Delta = r \cdot \delta w$, where r is a random number

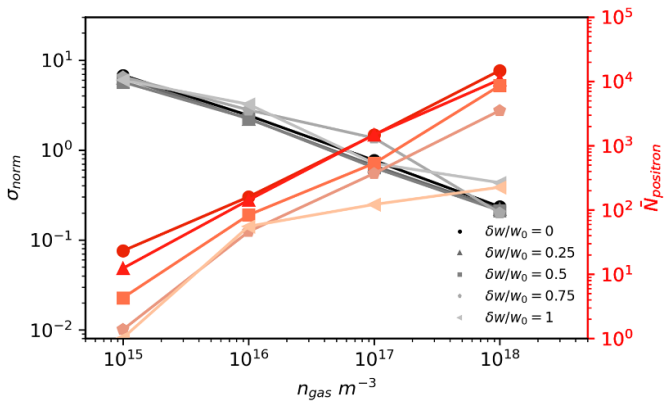

Figure 7. The normalized distributions' standard deviation σ and mean yield $\bar{N}$ versus different $n_{\rm gas}$ with laser transverse misalignment δw, the lasers' parameters are $a_0 = 1000$, $\tau_0 = 4T_0$ and $w_0 = 4\,\mu$m. Each point represents 1000 simulations. For $\delta w/w_0 = 1$ each point represents 3000 simulations due to low yields from large misalignment.

that follows a normal distribution. We simulate cascades for $\delta w = 0, 1, 2, 3, 4\,\mu$m and $w_0 = 4\,\mu$m. The results in figure 7 show that the average yields are suppressed when the misalignment increases since the number of electrons in the interaction region decrease when the two colliding pulses are misaligned. Although misalignment of laser spots adds extra randomness to the process, the trend of increased σ for lower gas densities remains. Moreover, as there is a trend of insufficient shots for statistics in figure 5 at lower density, the pointing instability requires more results to guarantee more reliable statistics. However, to better observe the effects, larger yields are preferred for a higher signal-noise ratio, and the laser misalignment should be well controlled.

4.3. The pre-pulse influences

For a PW laser system one must consider the influence of pre-pulses. For the investigated field strengths, the pre-pulses can fully ionize low-Z atoms like hydrogen, but relatively high-Z atoms (like oxygen and nitrogen) may only get partially ionized before the main pulse arrives. This effect has been discussed in several works such as [19, 22], in which the hydrogen/oxygen gas target is used for QED cascade. Since the pre-pulses are unable to fully ionize the inner-shell electrons, it is hard for the pre-pulses to sweep out the electrons in the interaction region. In a recent study on vacuum cleaning experiments [56] using pre-pulse-like lasers to ionize and eliminate the residual gas near the laser focus, it is found that while these ionized particles are pushed outward, a significant amount of residual particles also drift into the laser propagation path, indicating negligible effects of pre-pulses. The pre-pulses overall act as a modification of the gas densities near the laser focus, and increasing the gas density could compensate for the decrease in electrons.

5. Conclusion

In summary, we studied the seeded QED cascades driven by two counter-propagating laser pulses, and found that the positron yields follow specific distributions among multiple simulations, which reflects the stochastic nature of QED cascades. The quantum stochastic effect is greatly enhanced by the coupling between photon radiation and pair-production in the seeded cascade. The enhanced effect can be observed in the collision between ultra-intense laser pulses and thin gases, which are usually residual molecules in the vacuum chamber. The quantum stochastic effect can be quantified by the width of the distribution and exceptional events of the positron yields. Quantum effects are significant when the gas density is moderately low and the results become more deterministic at higher densities. For the experimental observation of quantum stochastic effects, a tightly focused laser is preferred and the pointing stability of the laser pulses should be well controlled for optimal yields. The proposed scheme can be validated with the 100 PW laser systems.

Data availability statement

No new data were created or analyzed in this study.

Acknowledgments

This work was supported by the CAS Project for Young Scientists in Basic Research (YSBR060), National Natural Science Foundation of China (11935008), the National Key Research and Development Program of China (2022YFE0204800), the International Partnership Program of Chinese Academy of Sciences (181231KYSB20200040), the China Postdoctoral Science Foundation (2022M713258) and the Shanghai Science and Technology Development Foundation (22YF1455100).

Conflict of interest

The authors declare that they have no known competing financial interests or personal relationships that could have appeared to influence the work reported in this paper.

ORCID iDs

Xuesong Geng https://orcid.org/0000-0003-1181-6518
Liangliang Ji https://orcid.org/0000-0002-7107-0626
Baifei Shen https://orcid.org/0000-0003-1021-6991

References

[1] Zhang Z *et al* 2020 The laser beamline in SULF facility *High Power Laser Sci. Eng.* **8** e4

[2] Emma C *et al* 2021 Free electron lasers driven by plasma accelerators: status and near-term prospects *High Power Laser Sci. Eng.* **9** e57

[3] Borneis S *et al* 2021 Design, installation and commissioning of the ELI-Beamlines high-power, high-repetition rate HAPLS laser beam transport system to P3 *High Power Laser Sci. Eng.* **9** e30

[4] Turner M, Bulanov S S, Benedetti C, Gonsalves A J, Leemans W P, Nakamura K, van Tilborg J, Schroeder C B, Geddes C G R and Esarey E 2022 Strong-field QED experiments using the BELLA PW laser dual beamlines *Eur. Phys. J.* D **76** 205

[5] Ritus V I 1985 Quantum effects of the interaction of elementary particles with an intense electromagnetic field *J. Russ. Laser Res.* **6** 497–617

[6] Zhang P, Bulanov S S, Seipt D, Arefiev A V and Thomas A G R 2020 Relativistic plasma physics in supercritical fields *Phys. Plasmas* **27** 050601

[7] Blackburn T G 2020 Radiation reaction in electron–beam interactions with high-intensity lasers *Rev. Mod. Plasma Phys.* **4** 5

[8] Gonoskov A, Blackburn T G, Marklund M and Bulanov S S 2022 Charged particle motion and radiation in strong electromagnetic fields *Rev. Mod. Phys.* **94** 045001

[9] Di Piazza A, Willingale L and Zuegel J D 2022 Multi-petawatt physics prioritization (mp3) workshop report (arXiv:2211.13187[hep-ph])

[10] Di Piazza A, Müller C, Hatsagortsyan K Z and Keitel C H 2012 Extremely high-intensity laser interactions with fundamental quantum systems *Rev. Mod. Phys.* **84** 1177–228

[11] Fedotov A, Ilderton A, Karbstein F, King B, Seipt D, Taya H and Torgrimsson G 2023 Advances in QED with intense background fields *Phys. Rep.* **1010** 1–138

[12] Bulanov S V *et al* 2011 Extreme field science *Plasma Phys. Control. Fusion* **53** 124025

[13] Jackson J D 1998 *Classical Electrodynamics* 3rd edn (Wiley)

[14] Breit G and Wheeler J A 1934 Collision of two light quanta *Phys. Rev.* **46** 1087–91

[15] Geng X S *et al* 2020 Spin-dependent radiative deflection in the quantum radiation-reaction regime *New J. Phys.* **22** 013007

[16] Li Y-F, Shaisultanov R, Hatsagortsyan K Z, Wan F, Keitel C H and Li J-X 2019 Ultrarelativistic electron-beam polarization in single-shot interaction with an ultraintense laser pulse *Phys. Rev. Lett.* **122** 154801

[17] Fedotov A M, Narozhny N B, Mourou G and Korn G 2010 Limitations on the attainable intensity of high power lasers *Phys. Rev. Lett.* **105** 080402

[18] Grismayer T, Vranic M, Martins J L, Fonseca R A and Silva L O 2017 Seeded QED cascades in counterpropagating laser pulses *Phys. Rev.* E **95** 023210

[19] Tamburini M, Di Piazza A and Keitel C H 2017 Laser-pulse-shape control of seeded QED cascades *Sci. Rep.* **7** 5694

[20] Duclous R, Kirk J G and Bell A R 2011 Monte Carlo calculations of pair production in high-intensity laser–plasma interactions *Plasma Phys. Control. Fusion* **53** 015009

[21] Elkina N V, Fedotov A M, Kostyukov I Y, Legkov M V, Narozhny N B, Nerush E N and Ruhl H 2011 QED cascades induced by circularly polarized laser fields *Phys. Rev. ST Accel. Beams* **14** 054401

[22] Sampath A and Tamburini M 2018 Towards realistic simulations of QED cascades: non-ideal laser and electron seeding effects *Phys. Plasmas* **25** 083104

[23] Efimenko E S, Bashinov A V, Bastrakov S I, Gonoskov A A, Muraviev A A, Meyerov I B, Kim A V and Sergeev A M 2018 Extreme plasma states in laser-governed vacuum breakdown *Sci. Rep.* **8** 2329

[24] Neitz N and Di Piazza A 2013 Stochasticity effects in quantum radiation reaction *Phys. Rev. Lett.* **111** 054802

[25] Wistisen T N, Di Piazza A, Knudsen H V and Uggerhøj U I 2018 Experimental evidence of quantum radiation reaction in aligned crystals *Nat. Commun.* **9** 795

[26] Ridgers C P *et al* 2017 Signatures of quantum effects on radiation reaction in laser-electron-beam collisions *J. Plasma Phys.* **83** 715830502

[27] Vranic M, Grismayer T, Fonseca R A and Silva L O 2016 Quantum radiation reaction in head-on laser-electron beam interaction *New J. Phys.* **18** 073035

[28] Harvey C N, Gonoskov A, Ilderton A and Marklund M 2017 Quantum quenching of radiation losses in short laser pulses *Phys. Rev. Lett.* **118** 105004

[29] Geng X S, Ji L L, Shen B F, Feng B, Guo Z, Yu Q, Zhang L G and Xu Z Z 2019 Quantum reflection above the classical radiation-reaction barrier in the quantum electro-dynamics regime *Commun. Phys.* **2** 66

[30] Gong Z, Hu R H, Yu J Q, Shou Y R, Arefiev A V and Yan X Q 2019 Radiation rebound and quantum splash in electron-laser collisions *Phys. Rev. Accel. Beams* **22** 093401

[31] Hu G, Sun W-Q, Li B-J, Li Y-F, Wang W-M, Zhu M, Hu H-S and Li Y-T 2020 Quantum-stochasticity-induced asymmetry in the angular distribution of electrons in a quasiclassical regime *Phys. Rev.* A **102** 042218

[32] Blackburn T G, Ridgers C P, Kirk J G and Bell A R 2014 Quantum radiation reaction in laser–electron-beam collisions *Phys. Rev. Lett.* **112** 015001

[33] Li J-X, Chen Y-Y, Hatsagortsyan K Z and Keitel C H 2017 Angle-resolved stochastic photon emission in the quantum radiation-dominated regime *Sci. Rep.* **7** 11556

[34] Guo R-T, Wang Y, Shaisultanov R, Wan F, Xu Z-F, Chen Y-Y, Hatsagortsyan K Z and Li J-X 2020 Stochasticity in radiative polarization of ultrarelativistic electrons in an ultrastrong laser pulse *Phys. Rev. Res.* **2** 033483

[35] Cole J M *et al* 2018 Experimental evidence of radiation reaction in the collision of a high-intensity laser pulse with a laser-wakefield accelerated electron beam *Phys. Rev.* X **8** 011020

[36] Poder K *et al* 2018 Experimental signatures of the quantum nature of radiation reaction in the field of an ultraintense laser *Phys. Rev.* X **8** 031004

[37] Bula C *et al* 1996 Observation of nonlinear effects in compton scattering *Phys. Rev. Lett.* **76** 3116–9

[38] Burke D *et al* 1997 Positron production in multiphoton light-by-light scattering *Phys. Rev. Lett.* **79** 1626–9

[39] Schwinger J 1951 On gauge invariance and vacuum polarization *Phys. Rev.* **82** 664–79

[40] Bell A R and Kirk J G 2008 Possibility of prolific pair production with high-power lasers *Phys. Rev. Lett.* **101** 200403

[41] Mironov A A, Gelfer E G and Fedotov A M 2021 Onset of electron-seeded cascades in generic electromagnetic fields *Phys. Rev.* A **104** 012221

[42] Grismayer T, Vranic M, Martins J L, Fonseca R A and Silva L O 2016 Laser absorption via quantum electrodynamics cascades in counter propagating laser pulses *Phys. Plasmas* **23** 056706

[43] Wu Y, Ji L and Li R 2021 On the upper limit of laser intensity attainable in nonideal vacuum *Photon. Res.* **9** 541

[44] Lobet M, d'Humières E, Grech M, Ruyer C, Davoine X and Gremillet L 2016 Modeling of radiative and quantum electrodynamics effects in PIC simulations of ultra-relativistic laser-plasma interaction *J. Phys.: Conf. Ser.* **688** 012058

[45] Gonoskov A, Bastrakov S, Efimenko E, Ilderton A, Marklund M, Meyerov I, Muraviev A, Sergeev A, Surmin I and Wallin E 2015 Extended particle-in-cell schemes for

physics in ultrastrong laser fields: review and developments *Phys. Rev.* E **92** 023305
[46] Guo Y, Geng X, Ji L, Shen B and Li R 2022 Improving the accuracy of hard photon emission by sigmoid sampling of the quantum-electrodynamic table in particle-in-cell Monte Carlo simulations *Phys. Rev.* E **105** 025309
[47] Salamin Y I and Keitel C H 2002 Electron acceleration by a tightly focused laser beam *Phys. Rev. Lett.* **88** 095005
[48] Luo W, Liu W-Y, Yuan T, Chen M, Yu J-Y, Li F-Y, Del Sorbo D, Ridgers C P and Sheng Z-M 2018 QED cascade saturation in extreme high fields *Sci. Rep.* **8** 8400
[49] Vranic M, Grismayer T, Fonseca R A and Silva L O 2016 Electron–positron cascades in multiple-laser optical traps *Plasma Phys. Control. Fusion* **59** 014040
[50] Jirka M, Klimo O, Bulanov S, Esirkepov T Z, Gelfer E, Bulanov S S, Weber S and Korn G 2016 Electron dynamics and γ and e^- e^+ production by colliding laser pulses *Phys. Rev.* E **93** 023207
[51] Sheng Z-M, Mima K, Sentoku Y, Jovanović M S, Taguchi T, Zhang J and Meyer-ter-vehn J 2002 Stochastic heating and acceleration of electrons in colliding laser fields in plasma *Phys. Rev. Lett.* **88** 055004
[52] Bulanov S V, Esirkepov T Z, Koga J K, Bulanov S S, Gong Z, Yan X Q and Kando M 2017 Charged particle dynamics in multiple colliding electromagnetic waves. Survey of random walk, Lévy flights, limit circles, attractors and structurally determinate patterns *J. Plasma Phys.* **83** 905830202
[53] Gonoskov A, Bashinov A, Gonoskov I, Harvey C, Ilderton A, Kim A, Marklund M, Mourou G and Sergeev A 2014 Anomalous radiative trapping in laser fields of extreme intensity *Phys. Rev. Lett.* **113** 014801
[54] Mironov A, Narozhny N and Fedotov A 2014 Collapse and revival of electromagnetic cascades in focused intense laser pulses *Phys. Lett. A* **378** 3254–7
[55] Bashmakov V F, Nerush E N, Kostyukov I Yu, Fedotov A M and Narozhny N B 2014 Effect of laser polarization on quantum electrodynamical cascading *Phys. Plasmas* **21** 013105
[56] Yu Q Q, Schlenvoigt H-P, Bock S, Shen B F, Sauerbrey R, Schramm U and Cowan E T 2021 Studying vacuum conditions for vacuum birefringence experiments *Matter, Material and Technology Workshop* (*Dresden, Germany*)